

Catechol as a Universal Linker for the Synthesis of Hybrid Polyfluorene/Nanoparticle Materials

Jonas Delabie, Ward Ceunen, Siebe Detavernier, Julien De Winter, Pascal Gerbaux, Thierry Verbiest, and Guy Koeckelberghs*



Cite This: *Macromolecules* 2021, 54, 4582–4591



Read Online

ACCESS |



Metrics & More

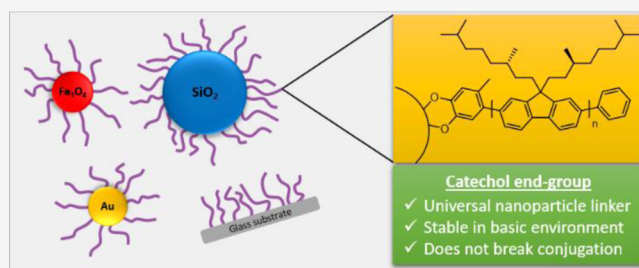


Article Recommendations



Supporting Information

ABSTRACT: The attachment of conjugated polymers (CPs), characterized by their optical and electronic properties and excellent processability, to inorganic nanoparticles (NPs), known for their specialized electronic and photonic properties, has proven to result in unique and promising (hybrid) materials. Although CPs can be functionalized with many different end groups, the process to find a correct match between the desired NP and appropriate functional group on the CP is often tedious and time-consuming. This study aims to solve this problem by investigating the potential of catechol as a universal linker molecule for the synthesis of hybrid CP/NP materials. First, the synthesis of poly(9,9-di((S)-3,7-dimethyloctyl)fluorene) via Suzuki–Miyaura catalyst transfer oxidative polycondensation using an external catechol Pd-initiator is investigated. A chain-growth polymerization without transfer reactions for molar masses up to 28.3 kg mol^{-1} is established without degradation of the catechol in basic environments. These polymers are subsequently used to graft a variety of NP materials, including magnetic- (Fe_3O_4), plasmonic- (Au), and oxide-type (SiO_2) NPs, proving its potential as a universal linker molecule. In addition, the influence of the catechol group on the supramolecular organization of free polyfluorene is investigated by comparison with the well-known *o*-tolyl end-capped polyfluorenes. From these results, it can be concluded that the catechol group significantly disrupts the formation of well-defined supramolecular architectures. Finally, as a preliminary study, the supramolecular organization of the hybrid NPs is compared to the free polymer using solvatochromism experiments. The results indicate an absence of chiral response upon fixation of the polymer onto a surface.



INTRODUCTION

Due to their light weight and promising conductive and optical properties, the potential application outreach for conjugated polymers (CPs) is seemingly unlimited. Apart from the well-known applications such as organic photovoltaics^{1–3} and polymer organic light-emitting diodes,^{4–7} CPs have shown great promise in applications using Faraday rotation^{8–10} and second- and third-order nonlinear optics.¹¹ Nevertheless, the potential of CPs has yet to reach its limit. This is proven by the recent evolution in which the optoelectronic properties and excellent processability of CPs are found to be a perfect match with the high electron mobility and unique photonic properties of inorganic nanoparticles (NPs). A wide variety of NPs such as TiO_2 , Fe_3O_4 , SiO_2 , and noble metals such as Au and Ag have all been used to make advanced hybrid CP/NP materials for the enhancement of optoelectronic devices^{12–16} or the development of theranostics,¹⁷ chemical tongues,¹⁸ and other sensing applications.^{17–22} However, each application requires a specific CP/NP combination, which in turn requires compatible, specific end-group functionalization of the CP. Although the CTCP mechanism allows for a wide variety of

functional end-groups such as amines,²³ thiols,²⁴ phosphonic acids,²⁵ cyanoacrylic acid,²⁶ and trialkoxysilanes,²⁷ the process of finding a suitable end group that must furthermore be compatible with the actual polymerization reaction (Murahashi, Kumada-Tamao, Negishi, Suzuki–Miyaura, Kosugi-Migita-Stille, etc.) is often very tedious and time-consuming (Figure 1).²⁸ In addition, the currently used linker molecules often break the conjugation, hindering the possibly desired charge transfer from the polymer to the NP, which limits the application outreach for these advanced hybrid materials. The demand for a convenient and consistent universal linker molecule that is capable of forming a stable organic–inorganic interface with many different NPs is therefore very high.

Received: February 18, 2021

Revised: April 14, 2021

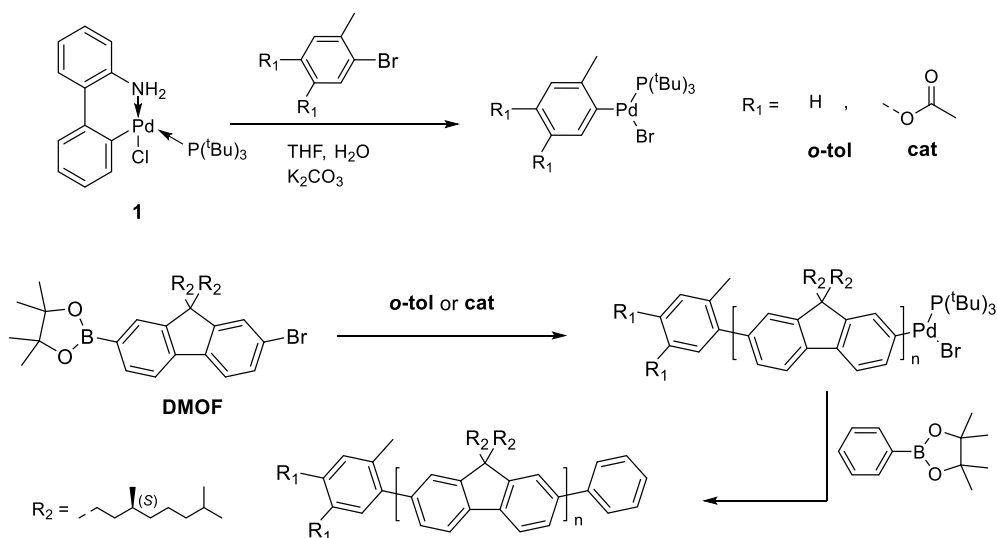
Published: May 5, 2021



Metal oxides and oxidized surfaces (SiO ₂ , TiO ₂ , ZnO, ITO, Al ₂ O ₃ , Fe ₂ O ₃ ,...)	Metals and Alloys (Au, Ag, Cd, CdSe, CdTe...)	Metals (Au, Ag, Pt, Cr...)
Universal linker molecule? 		

Figure 1. Examples of different linker molecules and their compatible surface material.

Scheme 1. Overview of the Suzuki–Miyaura Catalyst Transfer Condensation Polymerization of 9,9-Di((*S*)-3,7-dimethyloctyl)fluorene Using an External *o*-tol or *cat* Palladium Catalyst



This study aims to tackle this problem by introducing catechol-functionalized CPs as a universal end-group linker. When directly attached to the CPs, which is possible using CTCP in combination with an external catechol-based initiator, the catechol linker retains the conjugation. Small catechol-based molecules and some nonCPs have shown to bind to a variety of commonly used inorganic NPs such as CdS,²⁹ CdSe,²⁹ TiO₂,³⁰ Fe₃O₄,^{31,32} Au,³³ and ZnO.³⁴ In addition, we have already prepared a catechol-functionalized poly(3-alkylthiophene) using a Kumada CTCP (KCTCP) in combination with a catechol external initiator and have proven the formation of a stable coupling to magnetite (Fe₃O₄) NPs.³⁵ Although this approach was successful for this particular combination of polymers and NPs, there were some drawbacks, which potentially could hamper the deployment to other CPs using other CTCP reactions. First, the hydroxyl functions on the initiator need to be protected, as they react with the actual monomer in KCTCP (i.e., a Grignard reagent). While this drawback could be circumvented using other CTCP methods in which the hydroxyl function does not interfere with the polymerization, there is a second issue that cannot be solved by this approach. Previous research in our group revealed that during the initiator synthesis, oxidative insertion of the transition metal (Ni[PPh₃]₄ or a palladacycle) in catechol derivatives is

impossible due to the strong electron-donating nature of OH (in case of Ni[PPh₃]₄) or even O[−] (in case of the palladacycle—the reaction occurs in basic medium). As a consequence, the hydroxyl functions need to be converted to less electron-donating ester groups. Although this is by itself no severe restriction, this does require deprotection after polymerization. Because P3ATs, like all electron-rich CPs, are sensitive to acid, this must be done under basic conditions. To our surprise, this resulted in the decomposition of the catechol group (Figures S1–S2). This, evidently, is highly disadvantageous, as a less functional polymer can result in lower grafting densities or even inhibit NP functionalization completely. In an attempt to overcome this drawback, the deprotection was not done in a separate step, but in the presence of the NP, in the hope that some deprotected catechol binds to the NP prior to decomposition. However, if the catechol end group is ever to be used as a universal linker molecule, it is crucial that its stability in basic environments is demonstrated.

In this paper, the basic stability of catechol-functionalized polyfluorenes (PFs) is put to the test by synthesizing a CP using an external catechol initiator via a Suzuki–Miyaura CTCP (SMCTCP) mechanism. This particular reaction was chosen because the functionalized polymer is exposed under basic conditions not only in the post-polymerization

deprotection step, but also during the entire polymerization. Note that fluorene monomers are used for polymerization, as they polymerize more efficiently in SMCTCP compared to thiophenes. In addition, fluorenes also have increased aromaticity and are thus more stable compared to thiophene-based CPs. After the absence of transfer reactions during the SMCTCP with the external catechol initiator is investigated, the catechol-functionalized polymers are subsequently used to graft onto Au, Fe₃O₄, and SiO₂ NPs, covering plasmonic-, magnetic- and oxide-type NP materials. Furthermore, by using NPs of different sizes ranging from approximately 10 nm (Au and magnetite NPs) to 300 nm (SiO₂ NPs) and a flat surface (glass plate), the potential for a lot of different surfaces with different curvatures is covered. This is an important parameter, as it partly influences the proximity between the grafted polymer chains. Finally, a preliminary study is performed on the supramolecular behavior of catechol-functionalized poly(9,9-di-((*S*)-3,7-dimethyloctyl)fluorene)s grafted onto these NPs and onto a glass surface, as these properties are important for future applications.

RESULTS AND DISCUSSION

Influence of the Catechol Initiator on the Controlled Polymerization. It is the first time that an external catechol initiator is used in combination with SMCTCP. Because the catechol is much more electron rich compared to the often used *o*-tolyl initiator, quantitative generation of the external initiator could be hampered and it might also disturb the polymerization. Therefore, the influence of the *cat*-initiator in combination with the palladacycle (**1**) on the polymerization was investigated by plotting a series of monomers over initiator concentration ($[M]_0/[I]$) ratios in function of the obtained number average molar mass. The same experiment is performed on the usual *o*-tol initiator for comparison (Scheme 1). First, the *o*-tol or *cat* precursor catalysts are synthesized by reaction of the commercially available palladacycle (**1**) with 2-bromotoluene or acetyl-protected 4-methyl-catechol, respectively, after which they are added to solutions of DMOF in 3, 5, 8, 10, 15, 20, 25, and 30 $[M]/[I_0]$ ratios. Both the synthesis of the external initiator and the actual polymerization occur in the presence of aqueous K₂CO₃. Note that protection of the hydroxyl groups with acetyl groups is necessary because the polymerization takes place in basic environments, which could leave unprotected hydroxyl groups in a deprotonated state. As already mentioned, this increases the already strong electron-donating effect of the hydroxyl groups, which impedes the oxidative insertion of the precursor Pd catalyst into the C–Br bond of the catechol. After reacting overnight at RT, phenylboronic acid is added to the polymerization mixture to terminate the polymerization, yielding a series of *o*-tol-PF and *cat*-PF polymers. The molar mass dispersity (\mathcal{D}_M) and \bar{M}_n of the obtained polymers are analyzed using GPC analysis (Table S3). It is important to mention that these molar masses are overestimated, as the GPC is calibrated toward polystyrene standards. The presence of the catechol end group was also confirmed using ¹H NMR (Figure S4).

The obtained \bar{M}_n is plotted in function of the $[M]_0/[I]$ ratio for the series of *o*-tol-PF and *cat*-PF and is displayed in Figure 2. A linear relationship, indicating the absence of transfer reactions up to 24.5 and 28.3 kg mol⁻¹, is obtained for the polymerization of DMOF with *o*-tol and *cat*,

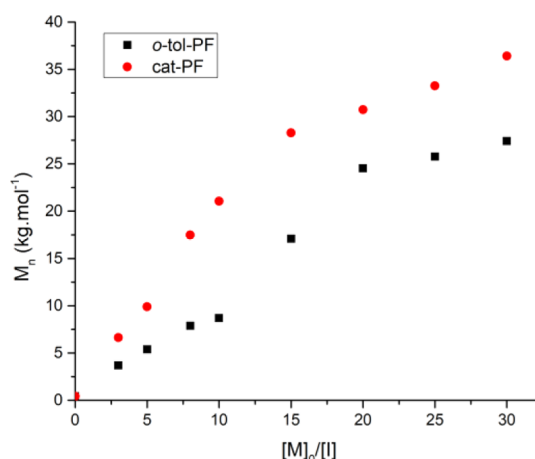


Figure 2. Overview of the $[M]_0/[I]$ ratio plotted against the obtained molar mass for both the *o*-tolyl (■) and catechol (●) catalysts for the polymerization of DMOF with SMCTCP.

respectively. The absence of transfer reactions is crucial because the polymer chains prepared after a transfer reaction will not be functionalized with the desired catechol moiety. Also, note that \bar{M}_n is consistently higher for *cat*-PF compared to *o*-tol-PF at the same $[M]_0/[I]$ ratio. This can be explained by partial degradation of the palladacycle into inactive Pd(0) during the formation of the *cat* and *o*-tol initiators. This decreases the amount of the active initiator before the polymerization, resulting in an increase of the actual $[M]_0/[I]$ ratio and thus a higher than expected \bar{M}_n . Although this degradation occurs for both initiators, it is larger for the *cat* initiator, leading to a consistently higher \bar{M}_n . This can be explained by the more electron-rich nature of the catechol, even with the protective groups, leading to a more difficult oxidative insertion of the palladacycle and thus a higher probability of catalyst degradation.

Besides consistently showing higher molar masses, the new *cat* initiator has little further influence on the polymerization of DMOF via SMCTCP, which is in contrast to the KCTCP of ((*S*)-3,7-dimethyloctyl)thiophene monomers with a catechol-based nickel initiator.¹⁰ Due to ring-walking over the conjugated chain, the catalyst can walk all the way back to the *cat* initiator at the α -end. This happens during both SMCTCP and KCTCP, however, KCTCP uses a Ni-catalyst, which has a larger affinity for the hard oxygen atoms of the *cat* initiator group compared to the softer Pd catalyst used in SMCTCP. This increases the probability of termination and transfer reactions compared to SMCTCP, explaining different influences of the *cat* initiator between both polymerization protocols.

Synthesis and Analysis of the Hybrid Materials. Now that the influence of the catechol on the polymerization is established, a new *Cat*-PF polymer with a \bar{M}_n of 12.9 kg mol⁻¹ (determined via GPC) is synthesized. MALDI-ToF MS and ¹H NMR analyses confirm the presence of the catechol end group (Figures S4 and S5). However, a fraction of the polymers appears to be end-capped on both sides, which is probably caused by disproportionation of the Pd catalyst toward the end of the polymerization. Nevertheless, the catechol group remained mostly present without signs of degradation, even after 16 h of polymerization in basic environment. Furthermore, due to the basic conditions, the hydroxyl groups are already deprotected during the polymer-

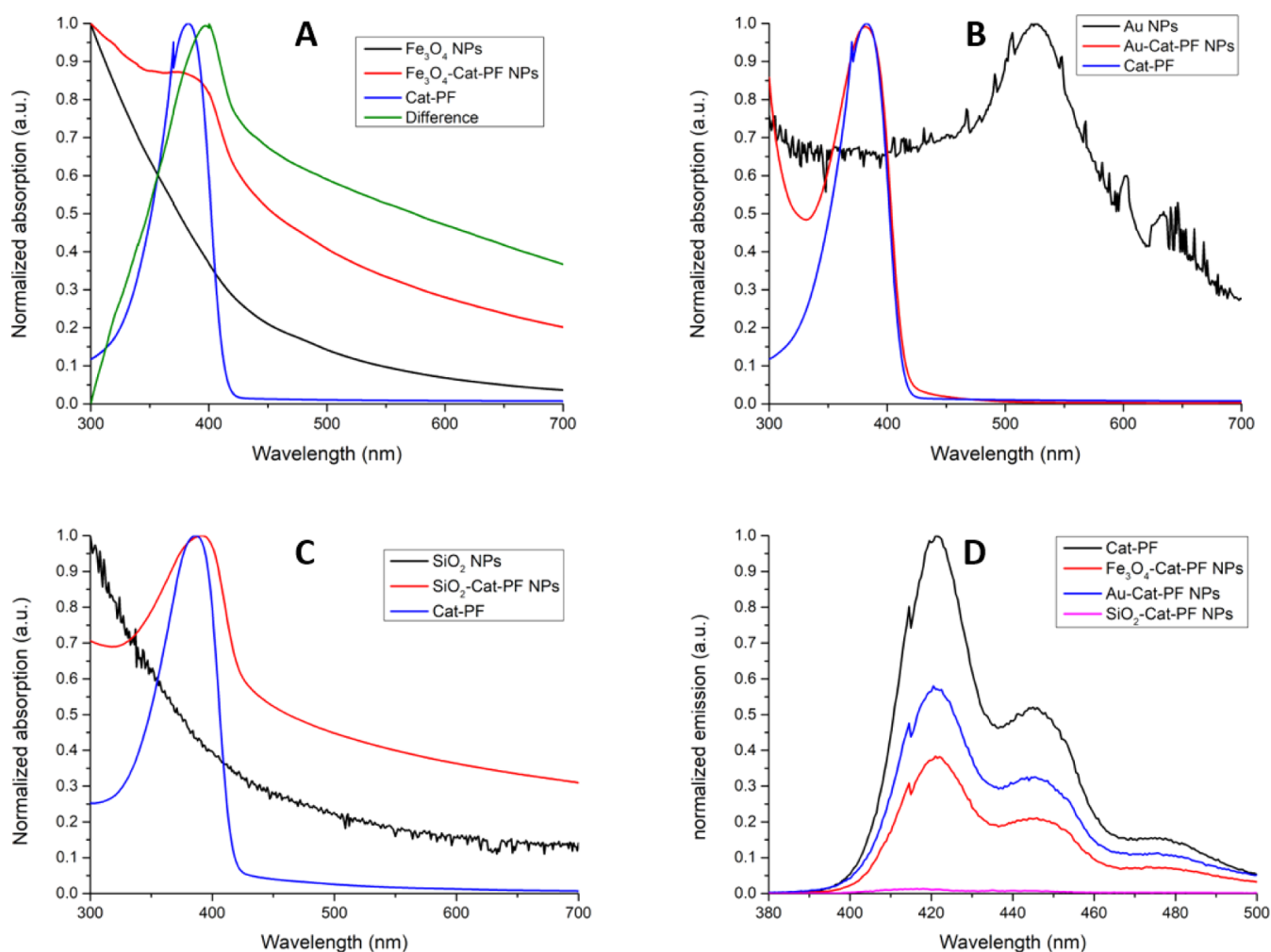


Figure 3. (A) Difference (green) between the UV-vis spectra of hybrid Fe₃O₄-Cat-PF NPs (red) and Fe₃O₄ NPs (black) compared to pure Cat-PF1 (blue). (B) UV-vis spectra of pure Au NPs (black), hybrid Au-Cat-PF NPs (red), and pure Cat-PF (blue). (C) UV-vis spectra of hybrid SiO₂-Cat-PF NPs (red) and SiO₂ NPs (black) compared to pure Cat-PF (blue). (D) Normalized and corrected emission spectra of Fe₃O₄-Cat-PF NPs (red), Au-Cat-PF NPs (blue), and SiO₂-Cat-PF NPs (pink) compared to pure Cat-PF (black).

ization, removing the need for a post-polymerization deprotection step. This is in large contrast to previous results obtained with catechol-functionalized P3AT, where complete degradation of the catechol functionality in basic environment was observed after only 3 h. It is important to note that this deprotection was done post-polymerization and is thus independent from the used polymerization mechanism. This means that catechol-functionalized P3AT is inherently unstable in basic environments, which implies that it cannot be synthesized using SMCTCP. Nevertheless, although complete deprotection of catechol-functionalized P3AT can never be obtained due to degradation, functionalization of the NPs is still possible via in situ deprotection.^{35,36} This implies that even for sub-optimal deprotection, the universal nature of the catechol group still applies.

After confirming the presence of the catechol functionality, this polymer is subsequently used to functionalize both Fe₃O₄, Au, and SiO₂ NPs according to adapted literature procedures, resulting in Fe₃O₄-Cat-PF, Au-Cat-PF, and SiO₂-Cat-PF hybrid NP materials, respectively.³⁵ The Fe₃O₄, Au, and SiO₂ NPs are spherical with a diameter of 10 ± 3, 11 ± 1, and 304 ± 19 nm, respectively, before functionalization

with Cat-PF, as determined by TEM and SEM analyses (Figures S7–S12). To ensure that no free polymer is present after the functionalization and before the investigation of the supramolecular organization, the hybrid magnetite NPs are purified using magnetic separation in THF. The free polymers remain in solution, while the hybrid NPs are retained by the magnet. This process is done repeatedly until a clear supernatant is obtained. The hybrid Au and SiO₂ NPs are purified using centrifugation, again until the supernatant is clear. To determine the success of the functionalization, the hybrid NPs are analyzed using UV-vis and fluorescence spectroscopy (Figure 3). The UV-vis analysis shows a very distinct polyfluorene peak after functionalization of the Au and SiO₂ NPs. For the Fe₃O₄-Cat-PF NPs, this peak is less obvious. However, the difference in UV-vis spectra before and after functionalization results in a spectrum that is in very close proximity to that of the free Cat-PF polymer. Note that for the Au-Cat-PF NPs, no absorption band that corresponds to Au NPs is observed on UV-vis. Nevertheless, TXRF analysis revealed that an average concentration of 1318 μg L⁻¹ of Au is present in the hybrid NP dispersion, confirming the presence of gold NPs (Table S4). Although UV-vis and TXRF analyses confirm both the presence of the inorganic

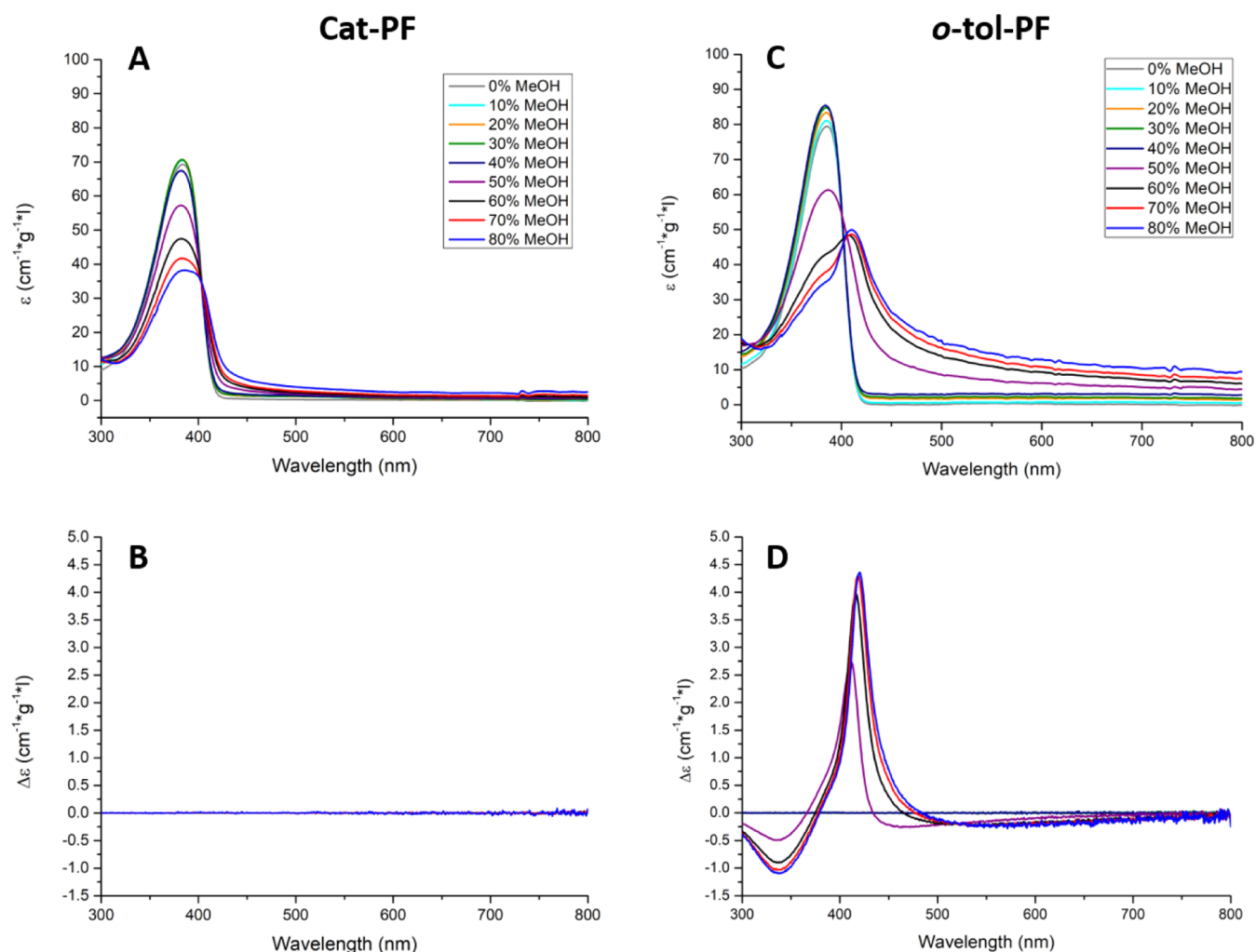


Figure 4. Overview of the UV-vis (A,C) and CD (B,D) analyses of the solvatochromism experiments of *cat*-PF and *o*-tol-PF starting with a concentration of 0.012 mg mL⁻¹ and 6.9 × 10⁻³ mg mL⁻¹ in CHCl₃, respectively, with MeOH as a nonsolvent.

NPs and the polymer after functionalization, additional fluorescence measurements are performed to prove that the *Cat*-PF is indeed grafted on the NPs. Figure 3D shows that the fluorescence is consistently quenched after functionalization of the NPs, which is a well-known side effect that occurs when CPs are grafted onto NPs.³⁷ Also, note how the fluorescence of the SiO₂-*Cat*-PF NPs is quenched significantly more compared to the other hybrid NPs. This can be explained by the larger size of the SiO₂ NPs, which translates in a smaller surface curvature compared to the other NPs. Consequently, there is a smaller angle between neighboring grafted polymers and thus a better interaction between the polymer chains, resulting in additional quenching due to nonradiative energy transfer. This proves that the polymer is indeed attached to the NP, confirming the successful synthesis of the hybrid materials. TEM and SEM measurements show that the spherical shape of the Fe₃O₄, Au, and SiO₂ NPs is perfectly retained after functionalization with *Cat*-PF, while the size has slightly increased. The diameters of the Fe₃O₄-*Cat*-PF, Au-*Cat*-PF, and SiO₂-*Cat*-PF hybrid NPs were found to be 16 ± 3, 14 ± 3, and 314 ± 19 nm, respectively. This small increase could be caused by the replacement of a small stabilizer molecule with the larger CP.

These results prove that the synthesis of catechol-functionalized CPs is indeed possible even in circumstances

that require long reaction times in basic environment. Furthermore, this catechol-functionalized PF is able to be grafted onto all kinds of NPs, ranging from plasmonic (Au NPs) to magnetic (Fe₃O₄ NPs) and even oxides (SiO₂ NPs) of different sizes. In addition, a flat glass substrate is grafted with *Cat*-PF to demonstrate how the utility of the catechol end group reaches beyond that of just NPs (Figure S13).

Supramolecular Organization of *Cat*-PF. Besides proving the universal nature of the catechol functionality, a preliminary study toward the supramolecular organization of grafted *Cat*-PF is performed. It is important to understand how these polymers organize when fixated to a NP or a substrate, as this gives rise to the most interesting properties of CPs.

Because previous research has shown how the organized aggregation behavior of CPs can be hampered simply by the end group,³⁸ first the influence of the catechol functionality on the supramolecular organization of polyfluorenes is investigated. This is done by comparing the solvatochromism experiments of *Cat*-PF with a very commonly used *o*-tolyl end-capped PF (*o*-tol-PF) of similar molar mass. *o*-tol-PF was synthesized as described above, but instead of catechol bromide, *o*-tolyl bromide was used in combination with the palladacycle (1) to obtain a *o*-tolyl-functionalized PF with a molar mass of 8.9 kg/mol, similar to *Cat*-PF (Figure S3).

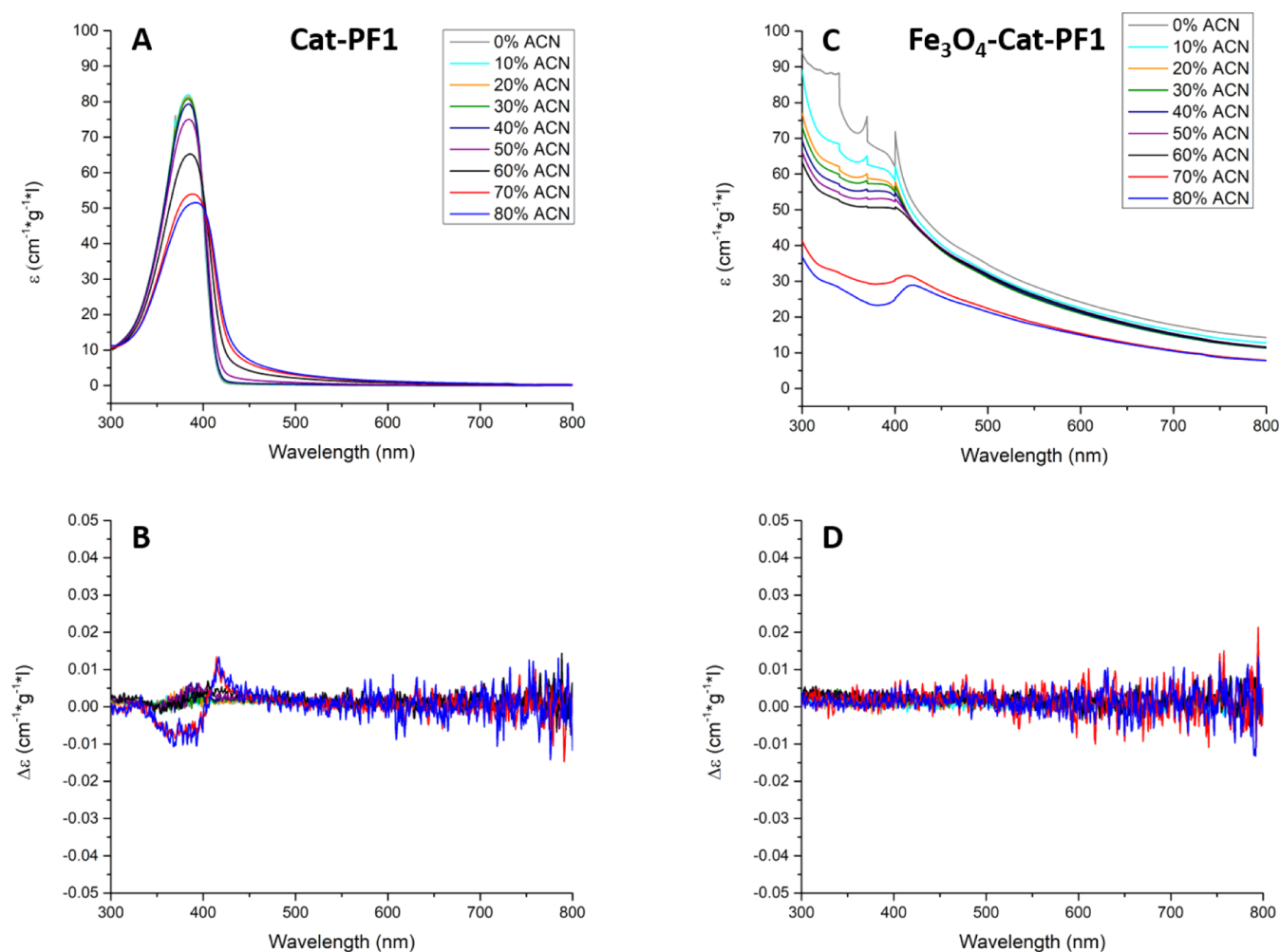


Figure 5. Overview of the UV–vis (A,C) and CD (B,D) analyses of the solvatochromism experiments of **Cat-PF** and **Fe₃O₄-Cat-PF** in **CHCl₃** with **ACN** as a nonsolvent.

The solvatochromism experiments are conducted by gradually adding a nonsolvent (MeOH) at a constant rate of 0.20 mL/min to polymer solutions of *o*-tol-PF and **Cat-PF** in **CHCl₃**. Subsequently, UV–vis and CD measurements are taken at 0, 10, 20, 30, 40, 50, 60, 70, and 80% MeOH concentrations (Figure 4). These results reveal a strong decrease in supramolecular organization of **Cat-PF** compared to *o*-tol-PF. While **Cat-PF** only shows a weak red shift and almost no CD signal, *o*-tol-PF displays a clear red shift and its corresponding CD signal starting from 50% MeOH. It can thus be concluded that the supramolecular organization of poly(9,9-di-((S)-3,7-dimethyloctyl)fluorene) is indeed hampered by the presence of a catechol group, which is in accordance with similar studies by Van den Eede et al.³⁸

Supramolecular Behavior of Hybrid NPs. Having established the influence of the catechol end group, the supramolecular behavior of the hybrid NPs can be investigated using solvatochromism experiments. Note that a different solvent system is used depending on the core NP material in order to have a minimal amount of precipitation upon the addition of nonsolvent. A chloroform (**CHCl₃**)/acetonitrile (**ACN**) system is used for the **Fe₃O₄-Cat-PF** NP and a THF/MeOH system for the **Au-Cat-PF** and **SiO₂-Cat-PF** NPs. As a reference, the hybrid material is always

compared with the corresponding free polymer under the same conditions.

First, the hybrid **Fe₃O₄-Cat-PF** and **Au-Cat-PF** NPs are studied. Figure 5 depicts the CD and UV–vis spectra of **Fe₃O₄-Cat-PF** and **Cat-PF**, where a red shift and a small CD signal is observed for **Cat-PF** starting from 60% nonsolvent concentrations. This is in contrast with the hybrid **Fe₃O₄-Cat-PF** NPs, which show no red shift nor a significant CD signal and thus no sign of (chiral) supramolecular organization. Similar results are obtained for the **Au-Cat-PF** NPs (Figure 6). A small red shift, accompanied with a small CD signal, is observed for the pure polymer starting at 60% MeOH, while for the hybrid **Au-Cat-PF** material, a small red shift is observed starting at 50% MeOH concentrations. However, at higher MeOH concentrations, extensive aggregation and flocculation of the hybrid NPs occur, leading to large amounts of scattering. Nevertheless, only a very small CD signal is obtained. These observations indicate that the fixation of catechol-functionalized PF onto the NPs hampers its supramolecular organization compared to the free polymer.

This corresponds well with previous research, which revealed how polythiophenes grafted onto NPs cannot form interchain interactions between polymer chains attached on the same NP.¹⁰ It was theorized that this is caused by the

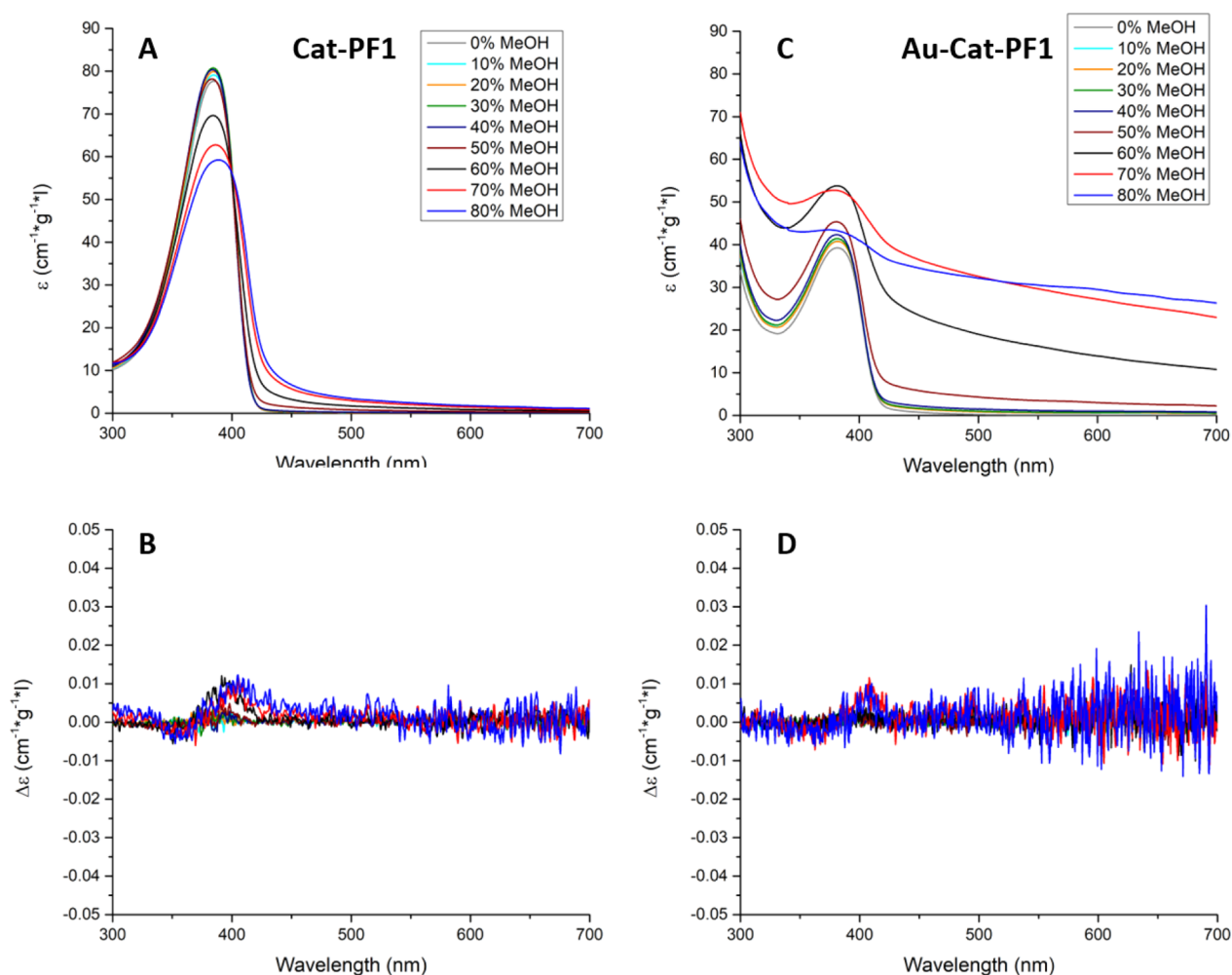


Figure 6. Overview of the UV–vis (A,C) and CD (B,D) analyses of the solvatochromism experiments of **Cat-PF** and **Au-Cat-PF** in THF with MeOH as a nonsolvent.

large curvature of the small magnetite NPs used (around 15 nm diameter), but this was never extensively studied. The curvature κ of a sphere is equal to the reciprocal of its radius r . Thus, by increasing the size of the NPs, the curvature becomes smaller with a limit of 0 m^{-1} for a flat surface. In theory, by using larger NPs and thus a smaller curvature, the angle between the grafted CPs can be reduced and might give rise to chiral organization.

In this section, the supramolecular organization of the previously synthesized large **SiO₂-Cat-PF** NPs ($314 \pm 19 \text{ nm}$) and the flat **Cat-PF**-grafted glass substrate is investigated and compared with the smaller **Fe₃O₄-Cat-PF** ($16 \pm 3 \text{ nm}$) studied earlier. This provides a spectrum of hybrid materials with different curvatures ranging from $1.25 \cdot 10^8 \text{ m}^{-1}$ for the **Fe₃O₄-Cat-PF** NPs and $6.3 \cdot 10^6 \text{ m}^{-1}$ for the **SiO₂-Cat-PF** NPs up to 0 m^{-1} for the **Cat-PF**-grafted glass substrate. **Figure 7** represents the UV–vis and CD analyses of the solvatochromism experiment performed on the **SiO₂-Cat-PF** NPs. However, once more no CD signal nor red shift is observed compared to the free polymer. Even for the flat **Cat-PF**-grafted glass substrate submerged in 100% MeOH, UV–vis is unaffected and also a chiral response remains absent (**Figure 8**). This means that even on a flat surface, there is no sign of any supramolecular organization.

Although it must be mentioned that the supramolecular organization of the free **Cat-PF** is already weak, all these observations indicate that the fixation of the **Cat-PF** onto a surface—whatever it is—hampers its supramolecular organization, despite the fact that fluorescence spectroscopy has shown that the polymer chains are indeed in close proximity. Combined with previous results, which were restricted to small NPs, this study suggests that attaching CPs to a surface destroys their (chiral) supramolecular organization.

CONCLUSIONS

In conclusion, poly(9,9-di-((*S*)-3,7-dimethyloctyl)fluorene) was successfully synthesized without transfer reactions up to 28.2 kg mol^{-1} (GPC, PS calibration) via SMCTCP using an external catechol-based initiator, resulting in a catechol end-capped polyfluorene CP. In contrast to preliminary results with catechol-functionalized poly(3-alkylthiophene), the catechol end group showed no signs of degradation during the polymerization in basic environments, opening up the possibilities for catechol end-group functionalization in countless other CPs. Furthermore, the catechol-functionalized PF was successfully used to graft onto a variety of NPs including magnetic- (**Fe₃O₄**), plasmonic- (**Au**), and oxide-type (**SiO₂**) NPs, proving its potential as a universal linker molecule. In addition, the influence of this catechol end

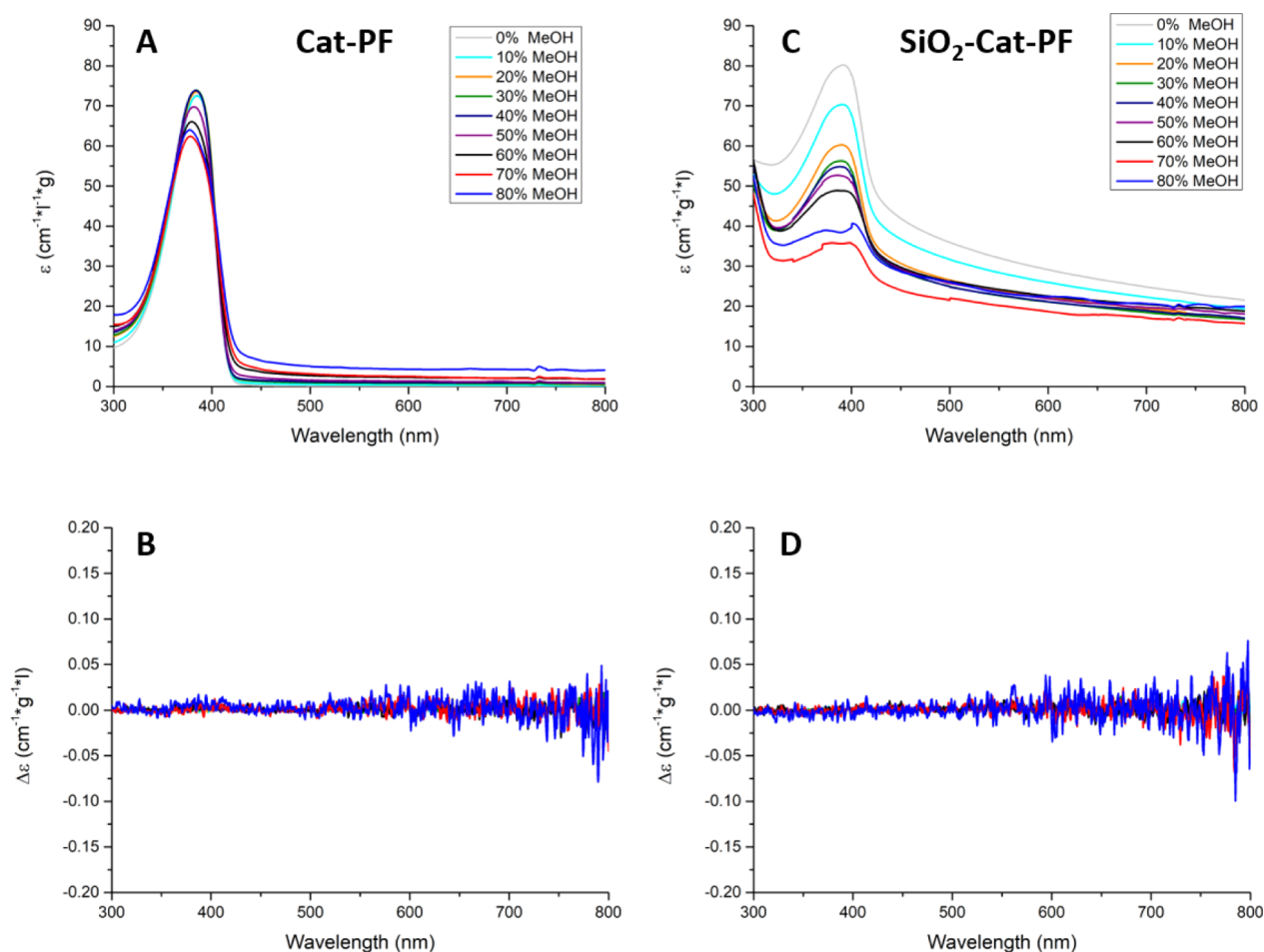


Figure 7. Overview of the UV-vis (A,C) and CD (B,D) analyses of the solvatochromism experiments of Cat-PF and SiO₂-Cat-PF in THF with MeOH as a nonsolvent.

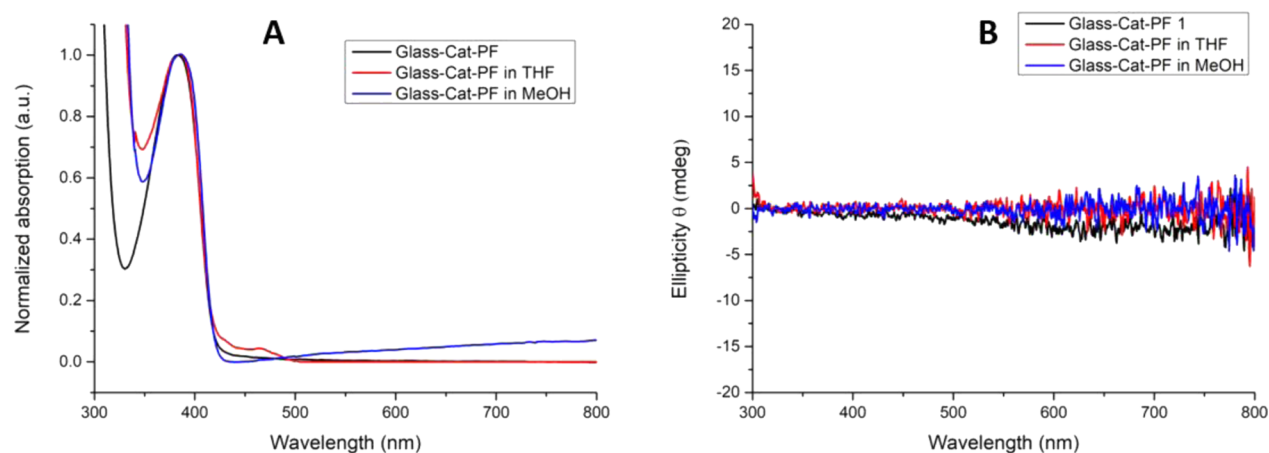


Figure 8. Overview of the UV-vis (A) and CD (B) analyses of Cat-PF grafted on glass substrates.

group on the supramolecular organization of polyfluorenes was investigated, and a significant disturbance was observed compared to regularly used *o*-tolyl end group-functionalized PFs. Finally, a preliminary study was performed concerning the supramolecular behavior of the PFs attached to hybrid NPs. Solvatochromism experiments were performed on hybrid NPs of different size and even a flat glass surface to investigate the influence of the curvature. Nevertheless, in all cases, no chiral response was observed, indicating a

disruption of the supramolecular organization, when the polymer is fixated onto a surface. This could possibly be explained by the reduced degrees of freedom of the CPs, preventing them from organizing in the most optimal way.

■ ASSOCIATED CONTENT

Supporting Information

The Supporting Information is available free of charge at <https://pubs.acs.org/doi/10.1021/acs.macromol.1c00386>.

Additional information about the materials and methods, ^1H NMR spectra, GPC spectra, MALDI-ToF analysis, additional UV-vis and CD spectra concerning the solvatochromism experiments, and TEM images of the NP materials (PDF)

AUTHOR INFORMATION

Corresponding Author

Guy Koeckelberghs – Laboratory for Polymer Synthesis, KU Leuven, B-3001 Heverlee, Belgium; orcid.org/0000-0003-1412-8454; Email: guy.koeckelberghs@kuleuven.be

Authors

Jonas Delabie – Laboratory for Polymer Synthesis, KU Leuven, B-3001 Heverlee, Belgium

Ward Ceunen – Laboratory for Polymer Synthesis, KU Leuven, B-3001 Heverlee, Belgium

Siebe Detavernier – Laboratory for Polymer Synthesis, KU Leuven, B-3001 Heverlee, Belgium

Julien De Winter – Organic Synthesis and Mass Spectrometry Laboratory, Research Institute for Materials Science and Engineering, University of Mons-UMONS, B-7000 Mons, Belgium; orcid.org/0000-0003-3429-5911

Pascal Gerbaux – Organic Synthesis and Mass Spectrometry Laboratory, Research Institute for Materials Science and Engineering, University of Mons-UMONS, B-7000 Mons, Belgium; orcid.org/0000-0001-5114-4352

Thierry Verbiest – Laboratory for Molecular Electronics and Photonics, KU Leuven, B-3001 Heverlee, Belgium

Complete contact information is available at:

<https://pubs.acs.org/10.1021/acs.macromol.1c00386>

Author Contributions

The manuscript was written through contributions of all authors. All authors have given approval to the final version of the manuscript.

Notes

The authors declare no competing financial interest.

ACKNOWLEDGMENTS

This research was funded by the Fund for Scientific Research (FWO-Flanders—1S04317N) and the Research Fund KU Leuven. J.D. is funded by FWO-SB. Arne Billen is acknowledged for the synthesis of the magnetite NPs, Kuo Zhong is acknowledged for the synthesis of the silica NPs, and Maarten Eerdeken is acknowledged for performing the TEM measurements. The MS lab is grateful to the “Fonds National de la Recherche Scientifique (FRS-FNRS)” for financial support for the acquisition of the Waters QToF Premier mass spectrometer.

REFERENCES

(1) Kim, Y.; Cook, S.; Tuladhar, S. M.; Choulis, S. A.; Nelson, J.; Durrant, J. R.; Bradley, D. D. C.; Giles, M.; McCulloch, I.; Ha, C.-S.; Ree, M. A Strong Regioregularity Effect in Self-Organizing Conjugated Polymer Films and High-Efficiency Polythiophene: Fullerene Solar Cells. *Nat. Mater.* **2006**, *5*, 197–203.

(2) Kim, J. S.; Wood, S.; Shoaee, S.; Spencer, S. J.; Castro, F. A.; Tsoi, W. C.; Murphy, C. E.; Sim, M.; Cho, K.; Durrant, J. R.; Kim, J.-S. Morphology-Performance Relationships in Polymer/Fullerene Blends Probed by Complementary Characterisation Techniques—Effects of Nanowire Formation and Subsequent Thermal Annealing. *J. Mater. Chem. C* **2015**, *3*, 9224–9232.

(3) Li, G.; Zhu, R.; Yang, Y. Polymer Solar Cells. *Nat. Photonics* **2012**, *6*, 153–161.

(4) Gross, M.; Müller, D. C.; Nothofer, H.-G.; Scherf, U.; Neher, D.; Bräuchle, C.; Meerholz, K. Improving the performance of doped π -conjugated polymers for use in organic light-emitting diodes. *Nature* **2000**, *405*, 661–665.

(5) Burroughes, J. H.; Bradley, D. D. C.; Brown, A. R.; Marks, R. N.; Mackay, K.; Friend, R. H.; Burns, P. L.; Holmes, A. B. Light-Emitting Diodes Based on Conjugated Polymers. *Nature* **1990**, *347*, 539–541.

(6) Heeger, A. J. Light Emission from Semiconducting Polymers: Light-Emitting Diodes, Light-Emitting Electrochemical Cells, Lasers and White Light for the Future. *Solid State Commun.* **1998**, *107*, 673–679.

(7) Gustafsson, G.; Cao, Y.; Treacy, G. M.; Klavetter, F.; Colaneri, N.; Heeger, A. J. Flexible Light-Emitting Diodes Made from Soluble Conducting Polymers. *Nature* **1992**, *357*, 477–479.

(8) Koeckelberghs, G.; Vangheluwe, M.; Doorselaere, K. V.; Robijns, E.; Persoons, A.; Verbiest, T. Regioregularity in Poly(3-Alkoxythiophene)s: Effects on the Faraday Rotation and Polymerization Mechanism. *Macromol. Rapid Commun.* **2006**, *27*, 1920–1925.

(9) Wang, P.; Jeon, I.; Lin, Z.; Peeks, M. D.; Savagatrup, S.; Kooi, S. E.; Van Voorhis, T.; Swager, T. M. Insights into Magneto-Optics of Helical Conjugated Polymers. *J. Am. Chem. Soc.* **2018**, *140*, 6501–6508.

(10) Ceunen, W.; Van Oosten, A.; Vleugels, R.; De Winter, J.; Gerbaux, P.; Li, Z.; De Feyter, S.; Verbiest, T.; Koeckelberghs, G. Synthesis and Supramolecular Organization of Chiral Poly-(Thiophene)-Magnetite Hybrid Nanoparticles. *Polym. Chem.* **2018**, *9*, 3029–3036.

(11) Vertommen, S.; Battaglini, E.; Salatelli, E.; Deschaume, O.; Bartic, C.; Verbiest, T.; Koeckelberghs, G. The Importance of Excellent π - π Interactions in Poly(thiophene)s To Reach a High Third-Order Nonlinear Optical Response. *J. Phys. Chem. B* **2020**, *124*, 9668–9679.

(12) Kim, K.; Carroll, D. L. Roles of Au and Ag nanoparticles in efficiency enhancement of poly(3-octylthiophene)/C60 bulk heterojunction photovoltaic devices. *Appl. Phys. Lett.* **2005**, *87*, 203113.

(13) Park, D. H.; Kim, H. S.; Jeong, M.-Y.; Lee, Y. B.; Kim, H.-J.; Kim, D.-C.; Kim, J.; Joo, J. Significantly Enhanced Photoluminescence of Doped Polymer-Metal Hybrid Nanotubes. *Adv. Funct. Mater.* **2008**, *18*, 2526–2534.

(14) Monson, T. C.; Hollars, C. W.; Orme, C. A.; Huser, T. Improving Nanoparticle Dispersion and Charge Transfer in Cadmium Telluride Tetrapod and Conjugated Polymer Blends. *ACS Appl. Mater. Interfaces* **2011**, *3*, 1077–1082.

(15) Zhang, Q.; Russell, T. P.; Emrick, T. Synthesis and Characterization of CdSe Nanorods Functionalized with Regioregular Poly(3-Hexylthiophene). *Chem. Mater.* **2007**, *19*, 3712–3716.

(16) Tu, Y.-C.; Lin, J.-F.; Lin, W.-C.; Liu, C.-P.; Shyue, J.-J.; Su, W.-F. Improving the electron mobility of TiO₂ nanorods for enhanced efficiency of a polymer-nanoparticle solar cell. *CrystEngComm* **2012**, *14*, 4772–4776.

(17) Barlas, F. B.; Aydinoglu, E.; Arslan, M.; Timur, S.; Yagci, Y. Gold nanoparticle conjugated poly(p-phenylene- β -cyclodextrin)-graft-poly(ethylene glycol) for theranostic applications. *J. Appl. Polym. Sci.* **2019**, *136*, 47250.

(18) Freudenberg, J.; Hinkel, F.; Jansch, D.; Bunz, U. H. F. Chemical Tongues and Noses Based upon Conjugated Polymers. *Top. Curr. Chem.* **2017**, *375*, 67.

(19) Wei, F.; Cai, X.; Nie, J.; Wang, F.; Lu, C.; Yang, G.; Chen, Z.; Ma, C.; Zhang, Y. A 1,2,3-triazolyl based conjugated microporous polymer for sensitive detection of p-nitroaniline and Au nanoparticle immobilization. *Polym. Chem.* **2018**, *9*, 3832–3839.

(20) Anantha-Iyengar, G.; Shanmugasundaram, K.; Nallal, M.; Lee, K.-P.; Whitcombe, M. J.; Lakshmi, D.; Sai-Anand, G. Functionalized Conjugated Polymers for Sensing and Molecular Imprinting Applications. *Prog. Polym. Sci.* **2019**, *88*, 1–129.

- (21) Lee, D.; Sin, D. H.; Kim, S. W.; Lee, H.; Byun, H. R.; Mun, J.; Sung, W.; Kang, B.; Kim, D. G.; Ko, H.; Song, S. W.; Jeong, M. S.; Rho, J.; Cho, K. Singlet Exciton Delocalization in Gold Nanoparticle-Tethered Poly(3-Hexylthiophene) Nanofibers with Enhanced Intrachain Ordering. *Macromolecules* **2017**, *50*, 8487–8496.
- (22) Yang, P.-J.; Chu, H.-C.; Lee, Y.-H.; Kobayashi, T.; Chen, T.-C.; Lin, H.-C. Quenching effects of gold nanoparticles in nanocomposites formed in water-soluble conjugated polymer nanoreactors. *Polymer* **2012**, *53*, 939–946.
- (23) Liu, J.; Tanaka, T.; Sivula, K.; Alivisatos, A. P.; Fréchet, J. M. J. Employing End-Functional Polythiophene To Control the Morphology of Nanocrystal–Polymer Composites in Hybrid Solar Cells. *J. Am. Chem. Soc.* **2004**, *126*, 6550–6551.
- (24) Palaniappan, K.; Murphy, J. W.; Sista, P.; Gnade, B. E.; Biewer, M. C.; Stefan, M. C. Poly(3-Hexylthiophene)-CdSe Quantum Dot Bulk Heterojunction Solar Cells: The Influence of the Functional End-Group of the Polymer. *Macromolecules* **2009**, *42*, 3845–3848.
- (25) Queffelec, C.; Petit, M.; Janvier, P.; Knight, D. A.; Bujoli, B. Surface Modification Using Phosphonic Acids and Esters. *Chem. Rev.* **2012**, *112*, 3777–3807.
- (26) Krüger, R. A.; Gordon, T. J.; Baumgartner, T.; Sutherland, T. C. End-Group Functionalization of Poly(3-Hexylthiophene) as an Efficient Route to Photosensitize Nanocrystalline TiO₂ Films for Photovoltaic Applications. *ACS Appl. Mater. Interfaces* **2011**, *3*, 2031–2041.
- (27) Lin, Y.-L.; Chu, J.-H.; Lu, H.-J.; Liu, N.; Wu, Z.-Q. Facile Synthesis of Optically Active and Magnetic Nanoparticles Carrying Helical Poly(Phenyl Isocyanide) Arms and Their Application in Enantioselective Crystallization. *Macromol. Rapid Commun.* **2018**, *39*, 1700685.
- (28) Bousquet, A.; Awada, H.; Hiorns, R. C.; Dagron-Lartigau, C.; Billon, L. Conjugated-Polymer Grafting on Inorganic and Organic Substrates: A New Trend in Organic Electronic Materials. *Prog. Polym. Sci.* **2014**, *39*, 1847–1877.
- (29) Singhal, P.; Maity, P.; Jha, S. K.; Ghosh, H. N. Metal-Ligand Complex-Induced Ultrafast Charge-Carrier Relaxation and Charge-Transfer Dynamics in CdX (X=S, Se, Te) Quantum Dots Sensitized with Nitrocatechol. *Chem.—Eur. J.* **2017**, *23*, 10590–10596.
- (30) Ooyama, Y.; Yamada, T.; Fujita, T.; Harima, Y.; Ohshita, J. Development of D- π -Cat fluorescent dyes with a catechol group for dye-sensitized solar cells based on dye-to-TiO₂ charge transfer. *J. Mater. Chem. A* **2014**, *2*, 8500–8511.
- (31) Thomas, A.; Bauer, H.; Schilman, A.-M.; Fischer, K.; Tremel, W.; Frey, H. The “Needle in the Haystack” Makes the Difference: Linear and Hyperbranched Polyglycerols with a Single Catechol Moiety for Metal Oxide Nanoparticle Coating. *Macromolecules* **2014**, *47*, 4557–4566.
- (32) Zhang, Q.; Nurumbetov, G.; Simula, A.; Zhu, C.; Li, M.; Wilson, P.; Kempe, K.; Yang, B.; Tao, L.; Haddleton, D. M. Synthesis of Well-Defined Catechol Polymers for Surface Functionalization of Magnetic Nanoparticles. *Polym. Chem.* **2016**, *7*, 7002–7010.
- (33) Son, H. Y.; Kim, K. R.; Hong, C. A.; Nam, Y. S. Morphological Evolution of Gold Nanoparticles into Nanodendrites Using Catechol-Grafted Polymer Templates. *ACS Omega* **2018**, *3*, 6683–6691.
- (34) Awada, H.; Mezzasalma, L.; Blanc, S.; Flahaut, D.; Dagron-Lartigau, C.; Lyskawa, J.; Woisel, P.; Bousquet, A.; Billon, L. Biomimetic Mussel Adhesive Inspired Anchor to Design ZnO@Poly(3-Hexylthiophene) Hybrid Core@Corona Nanoparticles. *Macromol. Rapid Commun.* **2015**, *36*, 1486–1491.
- (35) Ceunen, W.; Van Oosten, A.; Vleugels, R.; De Winter, J.; Gerbaux, P.; Li, Z.; de Feyter, S.; Verbiest, T.; Koeckelberghs, G. Synthesis and supramolecular organization of chiral poly-(thiophene)-magnetite hybrid nanoparticles. *Polym. Chem.* **2018**, *9*, 3029–3036.
- (36) Delabie, J.; De Winter, J.; Deschaume, O.; Bartic, C.; Gerbaux, P.; Verbiest, T.; Koeckelberghs, G. Development of a Layered Hybrid Nanocomposite Material Using α,ω -Bifunctionalized Polythiophenes. *Macromolecules* **2020**, *53*, 11098–11105.
- (37) Monnaie, F.; Verheyen, L.; De Winter, J.; Gerbaux, P.; Brullot, W.; Verbiest, T.; Koeckelberghs, G. Influence of Structure of End-Group-Functionalized Poly(3-Hexylthiophene) and Poly(3-Octylselenophene) Anchored on Au Nanoparticles. *Macromolecules* **2015**, *48*, 8752–8759.
- (38) Van Den Eede, M.-P.; Bedi, A.; Delabie, J.; De Winter, J.; Gerbaux, P.; Koeckelberghs, G. The Influence of the End-Group on the Chiral Self-Assembly of All-Conjugated Block Copolymers. *Polym. Chem.* **2017**, *8*, 5666–5672.